Original Research Paper

Volume - 11 | Issue - 08 | August - 2021 | PRINT ISSN No. 2249 - 555X | DOI : 10.36106/ijar

Chemistry

INVESTIGATIONS ON CHITOSAN/α-Fe_2O_3 NANOCOMPOSITE FOR EFFICIENT ANTIBACTERIAL ACTIVITY

M. Senthilkumar — Department Of Chemistry, Alagappa Chettiar Government College Of Engineering And Technology, Karaikudi-630 003. Tamil Nadu, India.

R. Pandimurugan — Department Of Chemistry, Ananda College Of Arts And Science, Devakottai-630 303. Tamil Nadu, India.

M. Muthuvinayagam* — Department Of Physics, School Of Advanced Sciences, Kalasalingam Academy Of Research And Education, India-626 190. *Corresponding Author

ABSTRACT Chitosan capped with α-Fe_2O_3 nanocomposite was prepared by simple chemical precipitation method. The synthesized Chitosan/α-Fe_2O_3 nanocomposite was characterised by FTIR, UV–visible spectroscopy and XRD analysis. These results showed that α-Fe_2O_3 nanoparticles were successfully grown on the surface of chitosan. The FTIR vibrational peaks confirm the blending between Chitosan and α-Fe_2O_3 nanoparticles. Ultraviolet-Visible absorption spectra explain the optical property of Chitosan/α-Fe_2O_3 nanocomposite. The sharp peaks in XRD pattern indicate the increase in crystallinity nature of Chitosan/α-Fe_2O_3 nanocomposite. Finally, the prepared Chitosan/α-Fe_2O_3 nanocomposite was tested for antibacterial activity against Staphylococcus aureus and Escherichia coli.

KEYWORDS : Chitosan/α-Fe_2O_3 nanoparticles; FTIR, XRD; UV-Visible; Antibacterial activity.

1.INTRODUCTION

The importance of nanomaterials and nanotechnology are increasing in modern science. Nanotechnology offers broad opportunities for scientists, engineers, physicians, chemists and physicists to achieve optimum results in the fields of health, biotechnology and many other areas of science and medicine[1]. As a consequence, nanomaterials particularly magnetic nanoparticles offer significant advantages due to their outstanding physicochemical properties and size, making them indispensable in numerous medical applications such as clinical diagnosis and therapeutic techniques[2–4].

Magnetic nanocrystals can exhibit many unique properties such as electrical, chemical, optical and magnetic properties[5-6] which are advantageous towards a variety of the applications. The three main types of iron oxide nanoparticles are FeO, Fe_2O_3 and Fe_3O_4. They are considered to be important materials due to their catalytic activity, biocompatibility, low-cost, nontoxicity and environmental friendly nature. Fe_2O_3, the ferric oxide has four crystallographic phases namely α-Fe_2O_3, β-Fe_2O_3, γ-Fe_2O_3 and ε-Fe_2O_3[7].

The synthesis of hematite particles(α-Fe_2O_3) in different sizes and shapes was thoroughly examined because of their new chemical and physical properties compared to bulk materials and their potential applications in inorganic pigments, catalysts, gas and humidity sensors, photoanode for photo electrochemical cells, photo electrolysis reactors, water treatment, lithium ion batteries and biological applications. Different techniques have been developed to synthesis hematite particles, such as polyol method[8], sol–gel method[9], spray pyrolysis [10], hydrothermal technique[11], chemical vapour deposition[12], pulsed laser deposition [13], co-precipitation and high vacuum evaporation[14]. In these synthesis methods, size and shape of the compounds change depending on the synthesis parameters, such as the reactant concentration, time and temperature reaction, pH solution, ionic strength, the anions, the surfactant and the nature of iron salts[15-17].

Polymers are emerged as the inevitable materials in daily life due to their applications in ever-growing industries such as medical, automobile, aerospace, electronics, packaging, food, photophysics and ferroelectrics[18]. These polymers are mostly non-degradable, leading to the harmful effect in the environment. C. J. Moore defines the ill-effect caused by the non-degradable polymers as “a rapidly increasing long-term threat”[19]. Therefore, the replacement of the non-degradable polymers by the suitable degradable biopolymers has gained much attention. Therefore, a list of bio-polymers such as cellulose, chitin, chitosan and poly amino acids are reported as the substitutes for the synthetic polymers in various applications[20]. However, chitosan is very much attractive than other bio-polymers owing to its bio-degradability, nitrogen richness, hydrophilicity, crystallinity, ionic conductivity and high viscosity. Chitosan is basically a linear polymer building up of 2- amino-2-deoxy-D-glucopyranose structural units that connected together by 1,4-glycosidic bonds. Chitosan is usually derived by the random N-deacetylation of chitin under alkaline conditions[21]. The inherent reactive amino groups of chitosan permit certain chemical modifications which lead to several important applications[22].

In this present study, we have prepared pure α-Fe_2O_3 nanoparticles and α-Fe_2O_3/Chitosan composites. They are characterized with Fourier Transform Infra-Red spectroscopy(FT-IR), Ultraviolet-Visible(UV-Vis) and X-ray diffraction(XRD). Then, the synthesized samples were tested for antibacterial activity against gram positive and gram negative pathogens.

2. MATERIALS AND METHODS

2.1 MATERIALS

All reagents used in the present investigation were analytical grade and used without further purification. Chitosan (average molecular weight of 180 kDa and 90% deacetylation) was purchased from M/s South India Sea foods, Kochi, Kerala, India. Iron (III) chloride (Sigma Aldrich) was the iron precursor, while sodium hydroxide was the precipitating agent, and ethanol (Sigma Aldrich) was used for washing. All solutions were prepared with distilled water.

2.2 Synthesis of Chitosan/α-Fe_2O_3 nanocomposite

In this procedure, Chitosan-Fe_2O_3 nanocomposite was prepared by dissolving 0.1M of iron (III) chloride in 100ml distilled water and the solution was stirred under magnetic stirring for 30 min at 80^{0}C. Then 0.1g of chitosan was dissolved separately in 25ml of acetic acid (5%), the solution was vigorously stirred for 30 min under magnetic stirrer. Now the iron (III) chloride solution was added in drop-wise. After stirring for 2h, freshly prepared 2M NaOH was used as the precipitating agent. Base solution (NaOH) was added gradually drop-wise to maintain a pH value of 11. The resulting precipitations were collected and centrifuged at 6000 rpm. Then it was washed with distilled water and ethanol for several times and finally dried in air at 80^{o}C. Thus, Chitosan-Fe_2O_3 nanocomposite was obtained. Similarly, pure Fe_2O_3 nanoparticles were prepared by this same procedure without adding chitosan.

2.3. Characterization techniques

The functional group determination was performed using Fourier transform infra red (FT-IR, SHIMADZU, using KBr pellets) spectroscopy in the range of 400–4000cm^{-1}. Powder X-ray diffraction study (XRD) was taken by XPert PRO PANalytical diffractometer. The Optical properties was measured using the Ultraviolet–Visible absorption spectral study (UV–Vis spectrum) carried out with Thermo scientific, Evolution 201 UV–Visible spectrophotometer and the fluorescence spectra were recorded in the wavelength range of 200–900 nm on JASCO spectrofluorometer (model: FP-8200).

2.4 Antibacterial test

The antibacterial activities were investigated against strains of gram positive microorganism Staphylococcus aureus(*S.aureus*) and strains

of gram negative microorganism Escherichia coli(*E. coli*). For qualitative measurements, the samples were put together to form a circular zone and the antimicrobial activity was tested using modified agar diffusion assay. The plates were kept at 37°C overnight incubation. After incubation, inhibition zone was measured with zone measurement scale. The diameter of the zone of inhibition was then examined directly underneath and around the sample. Particular zone in and around the sample was cleared and this determines the efficiency of the antibacterial agent to inhibit the growth of bacteria.

3. RESULTS AND DISCUSSION

3.1. FTIR Analysis

To confirm the binding mechanism, FTIR spectra of (a) Chitosan, (b) α-Fe_2O_3 and (c) Chitosan/α-Fe_2O_3 nanocomposite were examined as shown in *Fig. 1*. *In Fig. 1a*, a broad band found at 3422 cm^{-1} is due to the overlapped stretching vibration mode of O–H and N–H groups. The bands observed at 2921 and 2867 cm^{-1} are attributed to the CH_2 and CH_3 groups due to CH anti-symmetric and symmetric bands. The band at 2364 cm^{-1} is due to C–N asymmetric band stretching or may be due to carbon dioxide. The band at 1653 cm^{-1} is due to amide I band (C–O stretching along with N–H deformation mode) and at 1592 cm^{-1} is due to the characteristic peak of NH_2 group. Further, the FTIR spectrum of CH exhibits several characteristic bands such as 1375cm^{-1} is attributed to asymmetric C–H bending of CH_3 group, 1071cm^{-1} skeletal vibration involving the bridge C–O–C stretching of glucosamine residue and 1060–1015cm^{-1} bands corresponds to CH–OH in cyclic compounds[23].

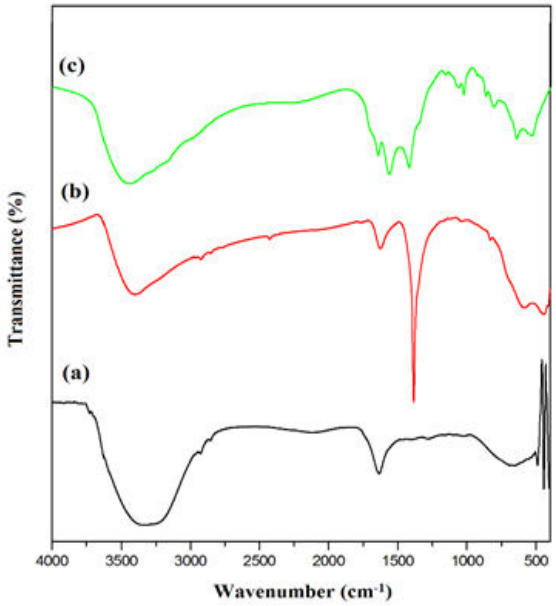

Figure 1. FTIR spectra of (a) Chitosan (b) α-Fe_2O_3 nanoparticles and (c) Chitosan/ α-Fe_2O_3 nanocomposite.

The FTIR spectrum of iron oxide nanoparticles shown in *Fig. 1b,* indicate the dominant bands at 466 and 568cm^{-1} which are the characteristics of crystalline Fe_2O_3[24]. The respective bands at 1160 and 1630cm^{-1} in nanoparticles are assigned to the symmetric stretching vibration of C–O–C group and bending vibration of water molecules[25]. The decrease in intensity of peak at 1160cm^{-1} reveals the removal of organic matter at higher temperatures. In the spectrum of Chitosan/α-Fe_2O_3 nanocomposite(*Fig. 1c*), the shifting of peak of N–H bending vibration to 1580cm^{-1} from the peak appeared at 1592cm^{-1} in the case of pure spectrum of CH indicated that the amine group of CH is involved in the assembling of Fe_2O_3 nanoparticles. The respective absorption bands of Fe_2O_3 nanoparticles appear at 536cm^{-1} and 428cm^{-1} belonging to the stretching vibration mode and the torsional vibration mode of Fe–O bonds in the tetrahedral sites and in the octahedral sites. These results indicated that CH was coated to the magnetic Fe_2O_3 nanoparticles successfully. It is because of the surface of iron oxide with negative charges that renders protonated CH to get attracted to the magnetite nanoparticles by the electrostatic interaction and chemical reaction in presence of glycolic acid as a cross-linking agent. The α-Fe_2O_3/Chitosan nanocomposite can not only modify the poor hydrophilicity but also provide the necessary active sites through which other biocompatible components such as proteins, polysaccharides, cell growth factors, or peptides can be further immobilized. To achieve the ionic coupling of bio-macromolecules, the CH was treated with a lesser amount of glycolic acid. The reaction between protonated NH_2 groups and OH–CH_2–COOH yielded a bonding via electrostatic, and one free polar group could react with another polar group existing in most bio-macromolecules such as CH, collagen, enzyme.

3.2. X-ray diffraction pattern

XRD analysis is the most useful technique for identification of crystalline structure of Chitosan and Chitosan/α-Fe_2O_3nanocomposites are shown in *Fig 2*. The X-ray diffractogram of Chitosan(*Fig. 2a*) has a broad peak around 11.2° in agreement with the characteristic diffractogram. The XRD patterns (*Fig. 2b*) show considerable line width as an indication of formation of particles having dimensions in the nanoscale. All the peaks in the pattern are indexed in accordance with the JCPDS-ICDD card number 89-0596 and the nanocrystals are observed to belong to the rhombohedral crystal system. The synthesized sample α-Fe_2O_3/Chitosan shows main characteristic peaks of α-Fe_2O_3 at 2θ values of 22.9°, 31.5°, 33.6°, 45.3°, 49.7°, 56.6°, 57.8°, 59.4°, 64.1°, 70.4°, and 75.4° corresponding to the reflections from the planes (0 1 2), (1 0 4), (1 1 0), (1 1 3), (0 2 4), (1 1 6), (0 1 8), (2 1 4), (3 0 0), (1 0 1) and (2 2 0) respectively. The absence of other peaks confirms the blending of the synthesized nancomposites.

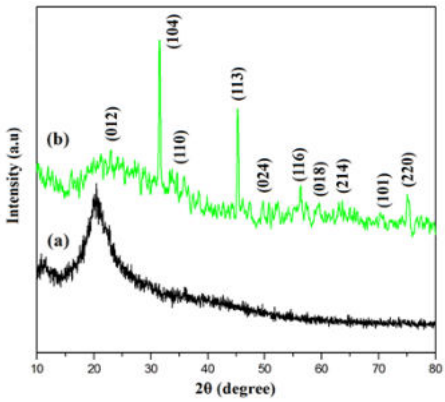

Figure 2. XRD pattern of (a) Chitosan and (b) Chitosan/α-Fe_2O_3 nanocomposite.

The average particle size of α-Fe_2O_3/Chitosan samples are 27nm determined by Scherrer diffraction formula (D = 0.94/βcosθ). This mainly depends on the influence of chitosan on Fe^{3+} ions.

3.3. OPTICAL ABSORPTION STUDY

In hematite α-Fe_2O_3-Chitosan samples, octahedrally coordinated Fe^{3+} ions show three types of electronic transitions: Fe^{3+} ligand field transitions (Fe^{3+} *d-d* transitions), ligand to metal charge-transfer (LMCT) transitions and transition arose from pair excitations of two magnetically coupled Fe^{3+}cations [26]. The absorption bands at 336nm, 529nm, 747nm and 850nm(*Fig.3*) are assigned to afore mentioned transitions. The absorption band at 336nm is due to transition from the ground $^6A_1(^6S)$ state to the excited $^4E(^4D)$ and $^4T1(^4D)$ ligand field states with combined LMCT transitions. The magnetic coupling of two adjacent Fe^{3+} cations exhibit the simultaneous excitation of two Fe^{3+} centers leading to a transition from a manifold ground $^6A_1(^6S)$ + $^6A_1(^6S)$ state to a coupled excited $^4T1(^4G)$+ $^4T1(^4G)$ state. This pair excitation transition and an overlapping of first band contribute to the strongest absorption at 529nm which is responsible for red colour of hematite. The weak absorption at 747nm is attributed to the $^6A_1(^6S)$ to $^4T_2(^4G)$ ligand field transition. Another ligand field transition between $^6A_1(^6S)$ and $^4T_1(^4G)$ states leads to an absorption at 850nm .

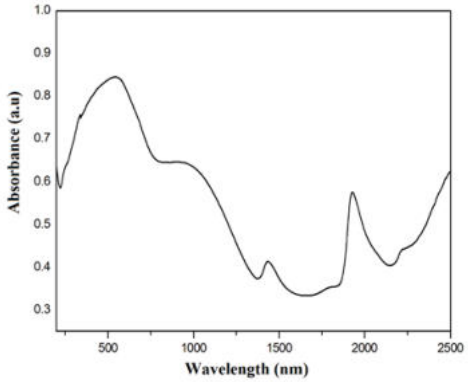

Figure 3. UV-Visible spectrum of Chitosan/α-Fe_2O_3 nanocomposite.

It is established that all of the transitions from the ground $^6A_1(^6S)$ state to the excited ligand field states are forbidden in terms of spin and parity. But in practice these transitions become allowed through pair excitation transitions from the simultaneous excitation of two neighbouring Fe^{3+}cations in the crystal structure that are magnetically coupled. In hematite nanocrystals, a few O^{2-} ions lie between the magnetically coupled Fe^{3+} ions, leading to an overlapping of Fe 3*d* and O 2*p* orbitals. Thus magnetic coupling of adjacent Fe^{3+} cations and covalent bonding with oxygen may relax some of the forbidden transitions. The influence of the covalent bonding may be modified by particle shape, size and morphology. Due to their large size (above 20nm) and lack of extensive surface modifications, significant shift is not observed in the optical absorption of the three different samples.

3.4. Antibacterial activity

The antibacterial activity of α-Fe_2O_3 and Chitosan/α-Fe_2O_3 nanocomposite was investigated against gram positive bacteria *S. aureus* and gram negative bacteria *E. coli*. The size of the zones of inhibition is shown in *Fig. 4* and value is mentioned in *Table 1*.

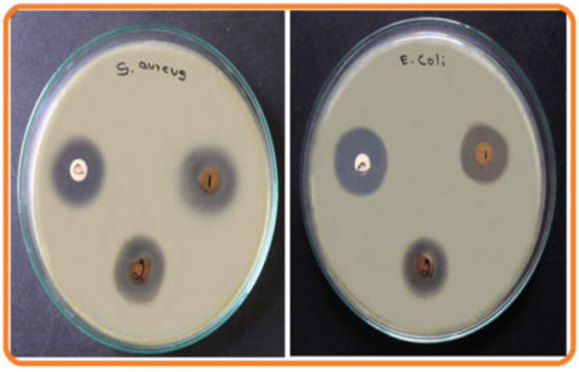

Figure 4. Photographs of the inhibition zone test of S.aureus and E.coli bactria. C = Control, 1 = α-Fe_2O_3 and 2 = Chitosan/α-Fe_2O_3 nanocomposite.

In general, the antibacterial activities of α-Fe_2O_3 nanoparticles towards bacteria and fungi depend on particle size, morphology, surface area, powder concentration, etc. α-Fe_2O_3 /Chitosan nanocomposite(30 lg/ml of concentration) has enhanced antibacterial activity than pure α-Fe_2O_3. The antibacterial activity of α-Fe_2O_3/Chitosan nanocomposite may not be entirely due to the metal alone. It may also due to the functional groups of amine in the chitosan. The formation of the zones around the samples demonstrated that the presence of α-Fe_2O_3 particles effectively prevent the growth of the two bacteria. Several mechanisms were proposed about antibacterial activity of the α-Fe_2O_3 nanoparticles applied for gram positive and gram-negative bacteria. One among these is, generation of reactive oxygen species like OH, O_2 and H_2O_2 on the surface of the α-Fe_2O_3 NPs, which cause a transfer of electrons from the valence band to the conduction band of the product material when α-Fe_2O_3 is irradiated with light having higher photon energy or energy equal to the band gap. By this process, the holes generated in the valence band can react with hydroxyl groups and absorb water to create hydroxyl radicals(OH). The electrons in the conduction band can be trapped by the presence of O_2 to produce superoxide radical anions (O_2) which in turn can react with hydrogen ions to form HO_2 radicals. The α-Chitosan/Fe_2O_3 nanocomposite samples having a small particle size (27nm) and low band gap energy have higher antibacterial activity than the other samples. Fe^{3+} interact with chitosan and attach to the cell wall, thus it disturbs cell wall permeability. To conclude, it is clear that Chitosan/α-Fe_2O_3 nanocomposite produce substantial yields of active α-Fe_2O_3 nanoparticles.

Table 1: The inhibition zone size values

Sample/Inhibition zone	*S.aureus* (mm)	*E.coli* (mm)
α-Fe_2O_3 nanoparticles	18 ± 0.36	20 ± 0.26
Chitosan/α-Fe_2O_3 nanocomposite	21± 0.42	25 ± 0.34

4. CONCLUSION

Chitosan/α-Fe_2O_3 nanocomposite was prepared by chemical precipitation method**.** These composites were analyzed using various analytical techniques. The interaction between α-Fe_2O_3 and Chitosan was investigated with the results of FT-IR. The XRD results show that the Chitosan/α-Fe_2O_3 nanocomposite has better crystallinity than that of Chitosan. Chitosan/α-Fe_2O_3 nanocomposite has particle size of 27nm and it was calculated using Scherrer diffraction formula from the XRD data. The optical property of Chitosan/α-Fe_2O_3 nanocomposite was indicated by UV-Vis spectra. Finally, the antibacterial activity of Chitosan/α-Fe_2O_3 nanocomposite was tested against gram positive and gram negative bacteria. The antibacterial activity of α-Fe_2O_3/Chitosan nanocomposite was greatly enhanced in comparison with α-Fe_2O_3 nanoparticles.

ACKNOWLEDGEMENT

Authors want to acknowledge the Department of Physics, Alagappa University, Karaikudi and CSIR-CECRI, Karaikudi, for their support to FT-IR and XRD studies.

REFERENCES

[1] A.L. Porter, J. Youtie, J. Nanoparticle Res. 11 (2009) 1023–1041.
[2] C. Corot, P. Robert, J.M. Idée, M. Port, Adv. Drug Deliv. Rev. 58 (2006) 1471–1504.
[3] Q.A. Pankhurst, J. Connolly, S.K. Jones, J. Dobson, J. Phys. D. Appl. Phys. 36 (2003).
[4] J. Dobson, Magnetic nanoparticles for drug delivery, Drug Dev. Res. 67 (2006) 55–60.
[5] M. Afrand, International Journal of Thermal Sciences. 118 (2017) 12-23.
[6] E.Dardan, M. Afrand, A.H. Meghdadi Isfahani, Applied Thermal Engineering. 109 (2016) 524–534.
[7] S. Sakurai, A. Namai, K. Hashimoto, S.-i. Ohkoshi, J. Am. Chem. Soc. 131 (2009) 18299-18303.
[8] D.W. Jung,D.W. Park , Appl Surf Sci (2009);255:5409–13.
[9] Lan F, Wang X, Xu X. . React Kinet Mech Catal (2012);106:113.
[10] Kim H, Pique A. Appl Phys Lett (2004);84:218–20.
[11] Zhang JR, Gao L. Mater Chem Phys (2004);87:10–3.
[12] Kim KS, Yoon SY, Lee WJ, Kim KH. Surf Coat Technol (2001);138:229–36.
[13] Thai TMN, Kim SR, Kim HJ. New Phys Sae Mulli 2014;64:252–5.
[14] Rinnert H, Miska P, Vergnat M, Schmerber G, Colis S, Dinia A, et al. Appl Phys Lett 2012;100. 101908(1)–101908(3).
[15] Nyir}o-Kósa I, Rec˘nik A, Pósfai M. Novel. J Nanoparticle Res 2012;14:1150–9.
[16] Ming M, Yu Z, Zhirui G, Ning G. Nanoscale Res Lett 2013;8:16–22.
[17] Ibrahim A, Abubakar AB. Afr J Pure Appl Chem 2013;7:114–21
[18] S. Mukherjee, H. Dinda, I. Chakraborty, R. Bhattacharyya, J. Das Sarma, R. Shunmugam, ACS Omega 2 (2017) 2848-2857.
[19] C. J. Moore, Environ. Res. 108 (2008) 131-139.
[20] S. Islam, M. R. Bhuiyan, M. Islam, J. Polym. Env. 25 (2017) 854-866;
[21] V. Zargar, M. Asghari, A. Dashti, ChemBioEng Rev. 2 (2015) 204-226.
[22] R. Antony, S. T. David, K. Saravanan, K. Karuppasamy, S. Balakumar, Spectrochim. Acta A 103 (2013) 423-430.
[23] F. Tian, Y. Liu, K. Hu, B. Zhao, J. Mater. Sci. 38 (2003) 4709–4712.
[24] V. Barron, J. Torrent, J. Colloid Interface Sci. 177 (1996) 407–410.
[25] C. Kormann, D.W. Bahnemann, M.R. Hoffmann, J. Photochem. Photobiol. A: Chem. 48 (1998) 161–169
[25] M. Sherman, T. D. Waite, Am. Miner. 70(1985) 1262-1269.
[26] Y. P. He, Y.M. Miao, C. R. Li, S.Q. Wang, L. Cao, S.S. Xie, G.Z. Yang, B.S. Zou, P h y s . Rev. 71 (2005) 125411–125419.